Development of Experimental Methods for Active Charge Control using Remote Sensing Methods

James Walker III[1] and Hanspeter Schaub[2]
Department of Aerospace Engineering Sciences University of Colorado Boulder

***Abstract*—Active charge control is being researched to tug, detumble or generally actuate a neighboring object. The electrostatic force and torque generation between a servicer and space object is referred to as the electrostatic tractor. Prior work has primarily researched this active charge control through simplified analysis or numerical modeling tools. This paper presents vacuum based experiments demonstrating the feasibility of controlling the potential using an electron gun and a touchless charge sensing methodology. A proportional controller is developed and applied to the energy of the electron beam. The secondary electron method, a novel remote sensing technique, is used to measure the target's electrostatic potential, which informs the feedback control. Previous research required the use of VUV lamps to fully control the potential of a target; however, it is shown in this paper that this can achieved using only an electron gun. In a vacuum chamber environment, for multiple charging scenarios, the control achieves the desired target potential within an accuracy of 10-50V. It is also found that, other than the gain, the speed of the secondary electron method is the most significant factor in determining the convergence time for each charging scenario. Finally, this control is shown to be robust to inconsistencies in the impact location of the electron beam on the target, an important property when the location of the electron beam is difficult to determine in realistic spacecraft scenarios.**

***Index Terms*—Spacecraft Charging, Active Charge Control, Secondary Electrons**

I. Introduction

Spacecraft charging occurs when environmental plasma impacts and accumulates on the surface of the spacecraft. Satellites in geostationary and cislunar orbits are especially vulnerable to charging because large fluxes of high energy electrons can cause spacecraft potentials to reach thousands of volts (in magnitude) [1]. Spacecraft with large electrostatic potentials can be hazardous to other spacecraft, especially during proximity and rendezvous operations: as charged spacecraft approach one another, they will exert significant Coulomb forces and torques on each other that can perturb their relative motion [2]–[4]. This effect is most significant when the separation distance between spacecraft is small, for instance during rendezvous or docking. Additionally, when the docking spacecraft have different electrostatic potentials, electrostatic discharges can occur that might damage the spacecraft [4].

While the aforementioned situations are a concern, control of spacecraft charging offers a unique opportunity for debris removal. The Electrostatic Tractor (ET) is a novel method for large debris removal that utilizes these electrostatic forces and torques [5], [6]. A servicing spacecraft directs a beam of high energy electrons at a debris object, applying a negative current and charging it to a negative potential [6]. Because the servicer is emitting negative particles, it experiences a positive current and charges accordingly. With these opposing charges, an attractive Coulomb force is generated between the two spacecraft [6]. This attractive force is the "Electrostatic Tractor" that allows the servicing spacecraft to influence the motion of the debris. Using low impulse thrusters, the servicer can tow the debris to a graveyard orbit where it no longer poses a threat to satellites in GEO orbits [7], [8]. This means a servicer spacecraft would be capable of contactlessly removing large debris objects from GEO orbits. It is found that, using the ET, a servicing craft can can re-orbit a multi ton debris object in a matter of months [9]. Fig. 1 shows an illustration depicting this process.

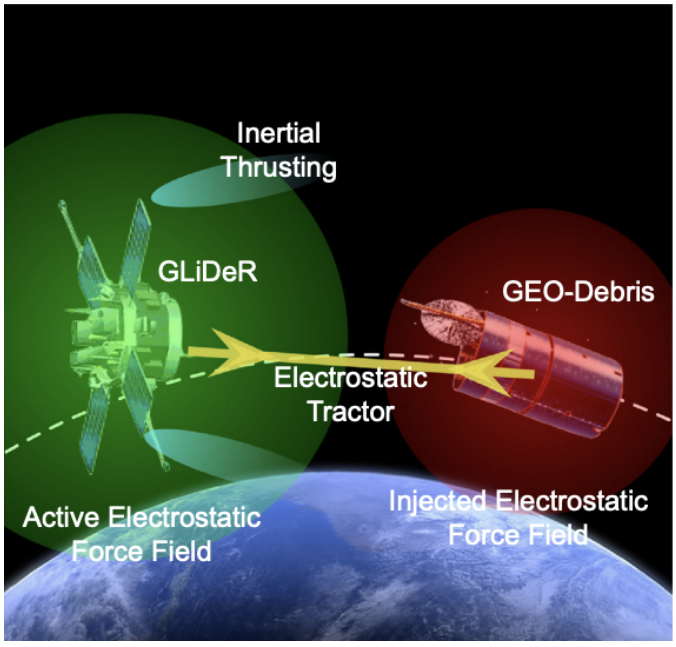

Fig. 1: Conceptual representation of servicer/debris configuration connected by Electrostatic Tractor [6].

One aspect this debris removal technique relies on is the ability of servicer to remotely measure the electric potential of the target. Two methods for remotely measuring a target's electric potential are the x-ray method and secondary electron

1: NDSEG Fellow, Graduate Research Assistant, Ann and H.J. Smead Department of Aerospace Engineering Sciences, Colorado Center for Astrodynamics Research

2: Professor and Department Chair, Schaden Leadership Chair, Ann and H.J. Smead Department of Aerospace Engineering Sciences, Colorado Center for Astrodynamics Research. AAS Fellow, AIAA Fellow

method (SEM) [10], [11]. Both these techniques involve a servicer irradiating a target with a high energy electron beam, exciting secondary electrons and x-rays from its surface [10], [11]. Secondary electrons are emitted with only a few eVs of energy [1] and are attracted toward the positively charged servicer where they impact with an energy equal to the potential difference between the two spacecraft [10]. The servicer measures the energy of the impacting electrons and, with a measurement of its own potential, determines the potential of the target [10]. On the other hand, as secondary electrons are emitted from the target surface, Bremsstrahlung radiation is generated. These x-rays will have a maximum energy equal to the difference between the target potential and electron beam energy impacting the target [11]. The servicer measures the energy of these x-ray photons and, knowing the energy of the electron beam and its own potential, the potential of the target is computed [11]. These methods have been experimentally researched in a vacuum chamber environment [10], [11].

The other important aspect of the ET is actively controlling the potential of the target. Previous implementations of active charge control have focused on a spacecraft controlling the potential of itself in order to improve measurement capabilities: to accurately measure electric fields and low energy electron and ion fluxes, a satellite must have a neutral charge. To achieve this, ion emitters are used to maintain near zero potentials when the spacecraft would otherwise charge positive, such as in sunlit regions or the magneto-tail lobes [12]–[16]. Electron beams as well as ion emitters have also been explored for active charge control, specifically in Coulomb formations [17]. By controlling the electric potential of each spacecraft in a Coulomb spacecraft formation, the relative motion of the swarm can be adjusted without using additional fuel [17]. In each of these cases, the servicer is controlling its own potential. This paper is concerned with touchlessly controlling the potential of a target object in a vacuum chamber environment. The idea of controlling a target's electrostatic potential has been discussed, specifically in terms of the ET [5], [6], but only preliminary experiments have been conducted. In Ref. 18, active charge control of a target is conducted using a high energy electron gun and VUV lamps in an idealized environment. An electrostatic voltmeter is used to measure the target's potential; however, this instrument requires a very small separation distance to function properly [18]. Regardless, it is shown that the electric potential of the target can be driven to a goal potential with an accuracy of 20V [18].

This paper focuses on developing and implementing active charge control in a more realistic scenario: incorporating remote sensing techniques, specifically the SEM, into the feedback controller. Additionally, as opposed to Ref. 18 where the electron current is controlled, it is determined that controlling the energy of the electron beam is more suitable for these experiments.

Section II details some of the underlying physics of the charging scenario presented here as well as the implementation of proportional controller. The experimental setup is outlined in Section III and the results of the experiments are presented in section IV. Section IV is outlined as follows. First, floating potential experiments are preformed to determine the potential induced by each beam energy. Next, the beam control is applied to multiple charging scenarios including varying initial beam energies, goal potentials, and gains. Finally, the limits of the current SEM are explored as they relate to this active charge control, specially in terms of convergence times and accuracy of measurements at high potentials.

Throughout this paper, unless otherwise specified, the electric potentials on the target are negative. When terms like "increasing" and "decreasing" are used relating to the target's potential, they are referring to the value's magnitude.

II. Numerical Methods

A. Overview of Spacecraft Charging

An electron gun emits a beam of energetic electrons. When directed at a target, the electrons impact its surface and stick, resulting in the target experiencing a negative current. However, this can only occur if the electric potential of the target, ϕ_T, relative to the potential of the servicer, ϕ_S, is less than the energy of emitted electrons, E_{EB}. If not, the electrons will not have enough energy to penetrate the electric field of the target and will be deflected away. The current applied to the target due to the impacting electron beam can be written as

$$I_T(\phi_T) = -\alpha I_{\text{EB}} \qquad \phi_S - \phi_T < E_{\text{EB}} \tag{1a}$$

$$I_T(\phi_T) = 0 \qquad \phi_S - \phi_T \geq E_{\text{EB}}, \tag{1b}$$

where I_{EB} is the current emitted from the electron gun and α is fraction of the beam impacting the target. For an accurate and focused beam, it is assumed the entire beam impacts the surface and α = 1. If there were no other currents acting on the target, then the electrons would continue to impact the target until its potential was equal to the energy of the electrons at which point, the beam electrons would be deflected away. However, even if environmental currents are ignored, like in vacuum chamber experiments, irradiating a target with electrons will cause additional currents.

Impacting electrons generate secondary and backscattered electrons. When a primary electron impacts a surface, it can transfer its energy to the surface electrons [1]. If enough energy is transferred, the surface electron will be emitted as a secondary electron [1]. When one secondary electron is emitted, there is no net current applied to the target as the primary electron adds a negative charge and the secondary electron removes a negative charge. However, the primary electron can share its energy with more than one surface electron, resulting in multiple secondary electrons and a net positive current on the target [1]. Secondary electron yield, represented by $\delta(E)$, is the ratio of secondary electrons to primary electrons. This yield is a function of E, the impact energy of the electrons. The impact energy is equal the difference between the energy of the primary electron and the target potential. The secondary electron yield is a unique material property that depends on a variety of factors including surface roughness, contamination layers, and incidence angle [1]. Figure 2 shows the secondary electron yield of pure aluminum with a normal incidence angle based on Ref. 19.

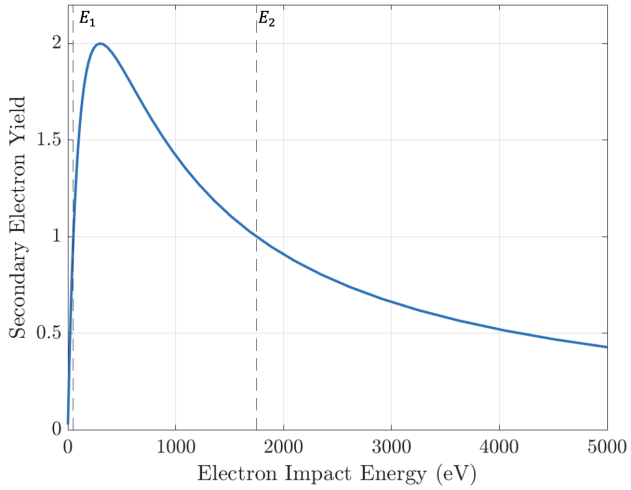

Fig. 2: The theoretical secondary electron yield for pure aluminum with a normal incidence angle according to Ref. 19. The dashed lines labeled as E_1 and E_2 are the first and second crossover energies.

The electron flux due to secondary electrons can be computed by using:

$$J_{\text{se}} = \int_0^\infty \delta(E) f(E) E \, \mathrm{d}E, \tag{2}$$

where $f(E)$ is the electron velocity distribution [1]. This secondary electron flux is the number of electrons emitted from a surface of unit area: given a specific surface, the secondary electron current, I_{se}, can be computed.

Backscattered electrons are also generated by primary electrons. Unlike secondary electrons, a backscattered electron never transfers energy to a surface electron. Instead, as it approaches the target, it is reflected, or backscattered, away [1]. This typically occurs around the ion sites of the material [1]. In this case, the backscattered electron is the same as the primary electron. Because of this, the backscattered yield, $\eta(E)$, cannot exceed 1. Similar to SEY, η is a material property that is a function of electron energy. The backscattered electron flux is given by Ref. 1 as

$$J_{\text{be}} = \int_0^\infty \eta(E) f(E) E \, \mathrm{d}E. \tag{3}$$

J_{be} can also be used to compute the current due to backscattered electrons, I_{be}, for a given surface. Because δ and η are both functions of E, they are often summed and referred to as the secondary and backscattered electron (SEEB) yield [1]. The backscattered electron yield is typically much smaller than the SEY and as such, the SEY and SEEB yield have very similar shapes.

Irradiating a target with an electron beam with a certain energy and current will result in the target charging to a floating potential that is determined by the SEEB yield. Referring to Fig. 2, there are two crossover energies where the total yield equals 1. At these equilibrium, the incoming and outgoing electrons are equal and the target potential remains constant:

$$I_{\text{net}} = -I_T + I_{\text{se}} + I_{\text{be}} = 0. \tag{4}$$

The first crossover energy, E_1 is an unstable equilibrium. If $E < E_1$, I_{net} is negative and the target charges negative. However, if $E > E_1$ for small deviations, then I_{net} is positive and the target will charge to near 0V. Any deviation from E_1 drives the potential away from the equilibrium point. The second crossover point, E_2, is a stable equilibrium. When $E > E_2$, the target charges negative and the impact energy decreases, until it reaches E_2. For small deviations, when $E < E_2$, I_{net} is positive. With the charge of the target increasing, the impact energy increases until it reaches E_2 and remains constant. For large deviations, the current is still positive, but the target will charge to a few volts positive. A more detailed explanation of this phenomenon is given Ch. 9 of Ref. 1. The electric potential the target charges to is referred to as the "floating potential" associated with that particular beam energy.

This charging effect allows the target to be discharged using only the electron gun. In Ref. 18, VUV lamps are used to apply a positive photoelectric current to the target and drive its potential to 0V. However, by adjusting the electron beam energy, a similar effect can be achieved. For a target with a negative potential, the impact energy of the electrons will be driven to E_2 [1]. Because E_2 is constant for the given setup, the difference between the electron energy and target potential also has to be constant: decreasing one will decrease the other by the same amount. This relationship can be used to drive the target to a near zero potential. Therefore, the target potential can be decreased using only the electron gun and these additional VUV lamps are not necessary. In this paper, $E \gg E_1$ as $E_1 < 300$eV for aluminum [19] and the minimum energy used here is 2000eV. Only the behavior around E_2 is relevant.

B. Electron Beam Energy Control

A proportional control is applied to the energy of the electron beam. For each electron energy, there is a floating potential that the target will achieve when irradiated (In Ref. 20, it is found that, for specific parameters, there are multiple floating potential, however this is not considered here). This floating potential occurs when the net current acting on the target is zero: the incoming and outgoing currents are equal. This control continually adjusts the electron energy until the floating potential is measured to be the same as the goal potential.

Two controllers are developed for this paper, a proportional (P) control and a proportional and derivative (PD) control. However, as shown by section IV, the proportional controller converges in relatively few iterations such that the derivative control is unnecessary and therefore not included. The P control, δV_P, is proportional to the error in the target's potential: the difference between the goal potential V_G and the measured target potential V_T,

$$\delta V_P = K_P (V_G - V_T), \tag{5}$$

where the proportional gain is K_P. The control is added directly to the beam energy. When the target potential is less than the goal potential, the difference is positive and the electron energy increases, driving the target potential closer to goal potential. When the difference is negative, the opposite occurs, but the control still drives this difference towards zero. When the measured potential reaches the goal potential, δV_P = 0, and the beam energy will remain constant. To protect the electron gun from damage by increasing the electron energy too quickly, a limit of δV_P = 1000eV is set.

III. Experimental Setup

Experiments are conducted in the Electrostatic Charging Laboratory for Interactions between Plasma and Spacecraft (ECLIPS) Vacuum Chamber in the Autonomous Vehicle Systems (AVS) lab at the University of Colorado at Boulder. The experimental setup includes a 4in aluminum cube mounted on a PEEK rod, an in-house built RPA, and a high energy electron gun. Figure 3 shows the experimental setup inside the vacuum chamber used for these experiments.

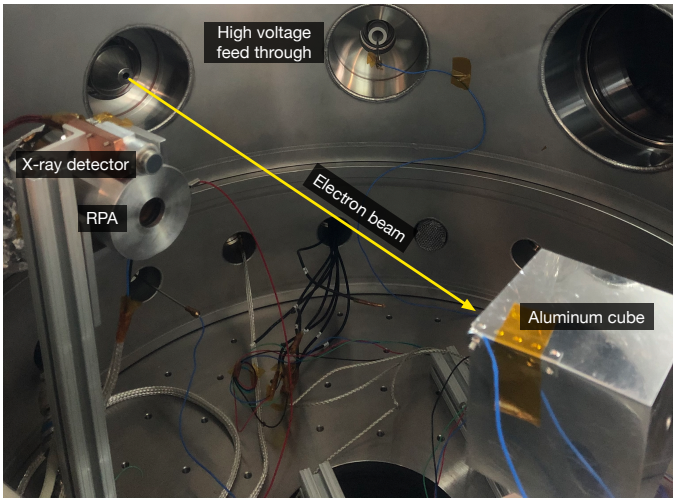

Fig. 3: The setup inside the ECLIPS vacuum chamber for active charge control experiments. [21]

The electron gun used throughout this paper is a Kimball Physics EGPS-4212B high energy electron gun with an energy range of 0eV - 30keV. This gun is operated in source mode, meaning the voltage across the source is held constant and the emitted current fluctuates as the energy of the gun changes. For all experiments, the current never drops below 5μA. As long as the current impacting the target is larger than the loss mechanisms (excluding SEEB) this decrease does not affect the charging behavior. These loss mechanisms include leakage current through the PEEK rod and field electron emission from the charge dense regions of the cube: the edges and the corners. These currents are orders of magnitude smaller than the emitted current.

The electron gun has the capability of adjusting the deflection of the beam. This allows for the location of the beam to be adjusted without changing the entire setup. However, this process uses electrostatics to deflect the beam and changing the electron energy changes the amount the beam is deflected. Before conducting the charge control experiments, the beam location is characterized using a phosphor screen to ensure the beam is accurate and focused at multiple energies. The phosphor screen illuminates blue when irradiated by electrons. By matching the illuminated regions at the different energies, there is high confidence that the beam is impacting at the same location at each beam energy.

A 4 inch aluminum cube is used to represent a spacecraft bus. An aluminum target is chosen for these experiments because aluminum is a common material used in spacecraft and its secondary electron yield has been relatively well characterized. However, the target used in this paper has a layer of oxide contamination that affects this yield. This shifts the E_2 value of the system, but because this setup is consistent for each charging scenario, it does not significantly affect the final results. In the vacuum chamber, the aluminum target is positioned at 18° relative to the electron gun. This allows the face of the target (where the electrons are impacting) to be normal to the inlet of the RPA, maximizing the number of secondary electrons accelerated into the RPA.

The SEM is used to measure the target's potential by measuring the energy of the secondary electrons that are emitted from the target when irradiated by an electron gun [10]. An RPA is used to determine the energy of the emitted electrons. Within the RPA are two grids: an external grid that is connected to ground and an internal grid that is connected to a high voltage power supply. When the electron gun is on, the target is irradiated and secondary electrons are generated. These secondaries are accelerated away from the now negatively charged target and into the RPA. A voltage sweep is conducted on the internal grid and current from the RPA is measured at every step. Once the potential on the internal grid is greater than the energy of the electrons, the electrons do not have enough energy to pass through the grid and the measured current drops significantly. By finding the largest drop in current, the potential of the target is found [10].

Because the SEM relies on a voltage sweep, the accuracy of the potential measurement depends on the step size of said voltage sweep. Two approaches to controlling the voltage sweep are presented in this paper. The first is to adjust the voltage sweep throughout each trial. Starting with a coarse voltage sweep and a wide energy range, the proportional controller converges to the desired potential with a poor accuracy. Then, the voltage sweep is refined, the voltage range reduced, and the control is allowed to converge again. This process is repeated until the control converges with the desired resolution. An example of this process for a goal potential of 1000V is as follows: the voltage range starts as 0V to 2500V with a step size of 500V. When the target potential is measured as 1000V, the range is adjusted to be 500V to 1500V with a step size of 100V. Once the control converges again, the SEM is adjusted to be from 900V to 1100V with a step size of 20V. The second approach to adjusting the SEM is to have it start with a wide range and small step size and run the control without adjusting it. In this case, the voltage sweep is constant throughout the entire the experiment. For instance, for a target potential of 4000V, the voltage is swept from 0V to 5000V with a step size of 50V. This SEM is used until the control

converges to the goal potential. In this paper, the smallest step size used is 20V.

The power supplies, multimeters, and other equipment are controlled remotely through a LabView interface; however, the energy input to the electron gun is manually controlled. Having the electron energy manually controlled prevents possible damage to the electron gun as abnormal energy values would be seen before input into the gun.

IV. Results

A. Floating Potentials

Before implementing the charge control, the value of E_2 for the system must be found. This value indicates the maximum beam energy that induces a 0V potential. Additionally, this allows for the target potential to be estimated using only the beam energy. Figure 4 shows the induced floating potentials for beam energies ranging from 0keV to 10keV.

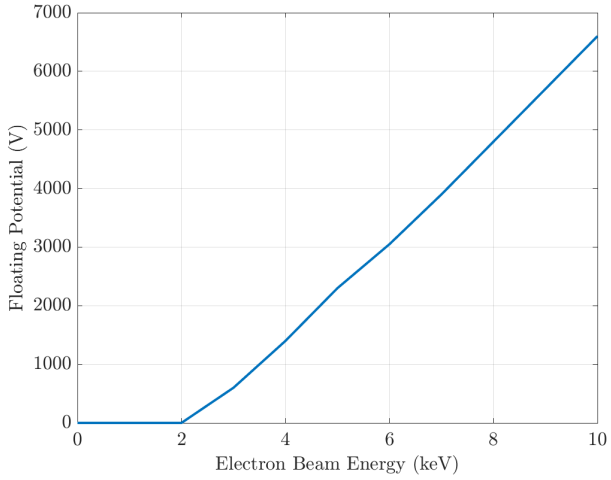

Fig. 4: The floating potentials of the experimental setup given beam energies ranging from 0keV to 10keV.

When the beam is at 3keV or higher, there is a relatively linear relationship between the target potential and beam energy. From this relationship, the E_2 value for this system is found to be 2950eV. Any beam energy lower than 2950eV does not significantly charge the target. Any energy greater than E_2 charges the target to approximately E_{EB} - E_2.

B. Feedback Control

The proportional controller described in Section II is implemented here. Figure 5 shows the target potential as a function time while undergoing active charge control. For this trial, the proportional gain is 0.2, initial beam energy is 5000eV, and goal potential is 1500V. The potential is found using the SEM with an intial voltage sweep range of 0V to 2500V and a step size of 100V. Within 2064s, the proportional control drives the target to, and maintains, the goal potential of 1500V within ±100V. After 2064s, the potential jumps to 1580V (indicated by the vertical line). Here, the step size of the SEM is reduced to 20V to improve the resolution. The range of the voltage

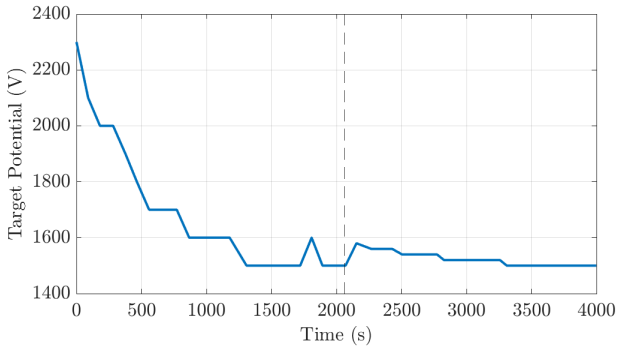

Fig. 5: The target's potential measured using the SEM when active charge control is applied to the beam energy. The vertical dashed line indicates when the voltage sweep of the SEM is adjusted.

sweep is also updated to be 1400V to 1600V to increase the speed of the measurements. After 3310s, the control converges again to 1500V but this time with a resolution of 20V.

Table I presents the charging behavior for each of the trials conducted for this paper. This includes initial potentials of 0V, 2300V, 2600V, 2950V, and 3950V and goal potentials ranging from 500V to 4000V. The resolution of the trial corresponds to the smallest resolution where the control could converge to a solution. For trials with $K_P \geq 1$ or constant SEM, the control does not converge for a resolution better than 50V. Finally, the last column indicates if the voltage sweep of the SEM is adjusted throughout the charging scenario or kept constant. In each scenario, the control is able to converge to the goal potential with a resolution of at least 50V.

In theory, a gain of 1 should result in perfect control: once the beam energy is greater than the second crossover energy, the relation between beam energy and target potential should be a one-to-one linear relationship [1]. Figure 6 shows that this is not the case. Here, two trials with gains of 0.5 and 1 and goal potentials of 1000V are presented.

With a gain of 0.5, the control converges in 794 seconds. Adjustments to the SEM are made at 264s and 680s: decreasing the width of the voltage sweep and reducing the step size.

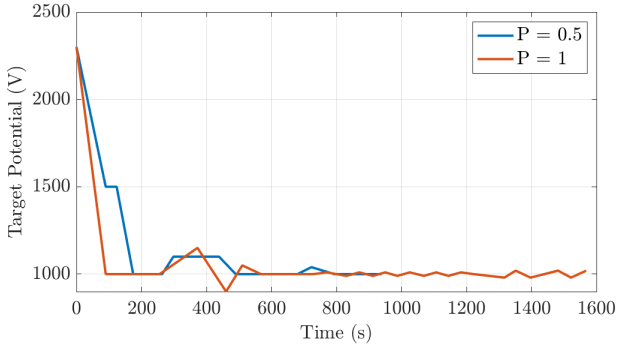

Fig. 6: The target's potential measured using the SEM when active charge control is applied to the beam energy with varying proportional gains.

TABLE I: Convergence behavior for active charge control scenarios.

Initial Potential (V)	K_P	Goal Potential (V)	Time to Steady State(s)	Resolution (V)	SEM
0	0.5	1000	940	50	Constant
0	0.5	4000	1055	20	Adjusted
2300	0.2	1500	3310	20	Adjusted
2300	0.5	500	648	20	Adjusted
2300	0.5	1000	794	20	Adjusted
2300	0.5	1000	1039	50	Constant
2300	1	1000	770	50	Adjusted
2300	2	500	1363	50	Adjusted
2600	0.75	1000	893	50	Constant
2950	0.5	1000	1506	50	Constant
3950	0.5	1000	2037	50	Constant

Using a gain of 1 yields more interesting results. With the initial coarse voltage sweep from 0V to 2400V and step size of 200V, the control converges to 1000V after one iteration. At 204s the voltage sweep is changed to be from 800V to 1200V with step size 50V. With the greater resolution, the voltage is measured to be 1150V. The control converges after some oscillations and the SEM is adjusted again at 729s to be from 950V to 1050V with step size 20V. For this voltage sweep, the grid potential of 1000V is not included which causes the potential to oscillate between 990V and 1010V. Even though the potential is not constant, there is only a $\pm$10V error. The final adjustments are made at 1183s where the sweep is changed to be from 940V to 1040V with step size 20V. Interestingly, the control still does not converge, it oscillates between 980V and 1020V and continues until the end of experiment.

There are two aspects found during the experiments shown in Fig. 6 that are interesting. First, it shows that a gain of 1 does not give perfect control. After the first time step, the target potential is measured to be 1000V, but it is actually at 1150V. This is not unexpected as the initial potential is only known to an accuracy of 200V. However, in the following time step, the target potential is driven to be 900V. If there was a one-to-one relationship between beam energy and target potential, the beam energy would drop 150V and the target would be measured to be 1000V with a resolution of 50V. Instead, decreasing the beam potential by 150V drops the target potential by 250V. This effect is likely do to inaccuracies in the pointing of the electron gun. Before running experiments, the impact location of the electron gun is matched for every 1000eV from 1keV to 10keV. The impact location of other beam energies will be slightly off center. Additionally, the shape of the electron beam is not consistent between energies. At lower energies, the spot size of the electron is large and circular. As the beam energy increases, the spot size shrinks and adopts an irregular shape. If the beam is impacting a different location, the incidence angle of the beam will not be consistent, resulting in an SEY that changes with beam energy. The E_2 will be different and the relationship between floating potential and E_2 will not be linear.

The second interesting aspect is that with a gain of 1, the control does not converge for a SEM resolution of 20V. This could be due to the issue described previously; however, for a difference of 20V, the change in deflection of the beam is going to be small enough such that the error in impact location should be negligible, especially at larger beam energies ($>$ 2000eV). If the target is at 1020V, the beam energy should decrease by 20eV and the target should be 1000V in spite of the small difference in impact location. As this is not the case, there is likely another cause: the SEM. The SEM has been shown to be accurate to within a few percent of the target's potential [22], [23]. In Ref. 22 specifically, it is shown that, for a potential of -511V, there is a 1.37% (7V) error. Assuming a similar error for the trials shown in Fig. 6, a 13V error is expected when the target is -1000V. This error is comparable to the SEM resolution and a control with a gain of 1 will have difficulty converging as the minimum energy change is 20V.

In spite of the of the inaccurate pointing of the beam and error in the SEM, gains are still chosen that allow the control to achieve the goal potentials with a resolution of 20V.

For the adjusted trials, like those presented in Figs. 5 and 6, the voltage sweep of the SEM is reconfigured throughout the charging scenario. Each step of the voltage sweep in the SEM can take up to 6s and each sweep typically has 10 steps. This allows for the control to converge in a reasonable amount of time and still achieve a good resolution. However, there are some drawbacks to this method: it requires additional control, but more importantly, if there is a change in the charging scenario, the SEM will not be able to accurately measure the target's potential. For the final resolution of 20V, the limits of the voltage sweep are V_G $\pm$100, meaning no potential outside this range can be accurately measured. Having a constant SEM increases the time it takes to measure, but allows for a wider range of potentials to be measured at any given time.

Figure 7 shows active charge control trials where the SEM is not adjusted; the voltage is swept from 0V to V_{max} with a step size of 50V. Trials 1 and 2 have a V_{max} = 2500V. For trials 3 and 4, V_{max} is 3000V and 4000V respectively. A gain of 0.5 and a goal potential of 1000V are selected for each trial. To achieve a starting potential of 0V for trial 1, a beam energy of 2000eV is used.

Trials 1 and 2 converge to the goal potential after 940s and 1039s respectively. These times are comparable to the convergence times seen in Fig. 6; however, in Fig. 7 the resolution is only 50V. Achieving a resolution of 20V would take 2.5$\times$ longer. Trials 3 and 4 converged after 1506s and 2037s, respectively, but this is not surprising. Because these trials have larger ranges for the voltage sweep, more steps of

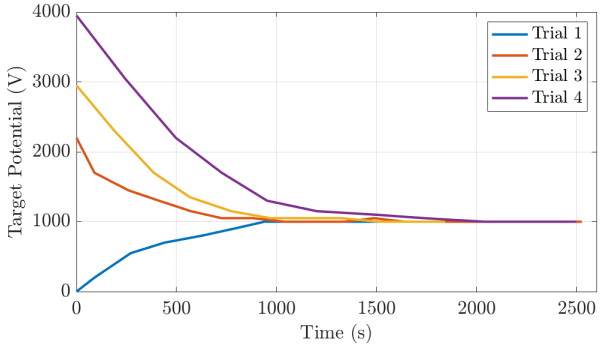

Fig. 7: The target's potential with active charge control driving the potential to 1000V with an unchanging voltage sweep.

the SEM are conducted, leading to longer convergence times. For a constant SEM, increasing the voltage range significantly increases the convergence time as more steps of the SEM are required. In contrast, with an adjusted SEM, the convergence time should be similar regardless of the range. This is shown in Fig. 9 where the voltage sweep is from 0V to 5000V, but the control still converges in 1055s.

Figure 8 shows the active charge control driving the target to -4000V. The initial voltage sweep is from 0V to 4250V with a step size of 250V. At 798s, the potential seems to jump from

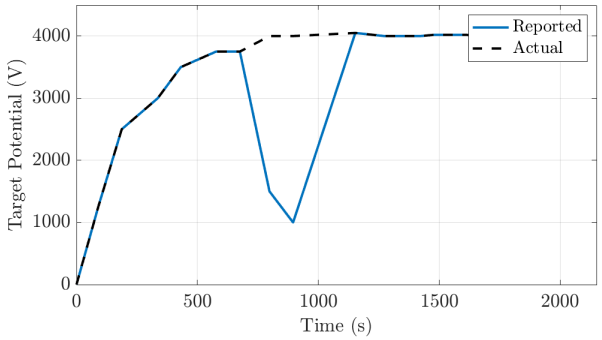

Fig. 8: The target's potential measured using the SEM with active charge control driving the potential to -4000V. The dashed line indicates the actual target potential while the solid line indicates the values reported by the SEM.

3750V to 1500V in one time step. The potential of the target does not actually change at this time step, the SEM outputs the wrong the value. A second measurement of the potential (without adjusting the energy) at 896s shows that this is a consistent error. At 1153s, the range of the voltage sweep is adjusted to be from 3500V to 4200V. With the reduced range, the correct potential is measured. As discussed in section III, the SEM measures the target's potential by measuring where the largest drop in current occurs. At 1500V, the current drops from 5.1nA to 4.5nA, a drop of 0.63nA. However, the current decreases from 0.61nA to 0.11nA at 4000V, a drop of 0.51nA. Even though the drop at 4000V is more significant, the current decrease is larger at 1500V because the current magnitudes are larger. This causes the SEM to report incorrect values when measuring target potentials larger than 2000V. The dashed line in Fig. 8 shows the actual target potentials, found by examining the data at these outlying points. To correct this, the SEM is altered such that the indicator of the potential is the maximum drop in current relative to the measured current. At 4000V, this value is 0.82 while at 1500V, it is 0.12. Implementing this version of the SEM requires an accurate measure of the noise floor. If values below this threshold are considered, it can result in false measurements. For example, the noise may jump from -1e-12A to 1e-12A and, while this is clearly due to noise, the percent change would be 200%, larger than any other percent change. Ignoring values below the noise floor avoids this issue.

Figure 9 shows the same scenario presented in Fig. 8 with the corrected SEM implemented. This corrected SEM is also used to measure the potentials of Trial 3 and 4 shown in Fig. 7.

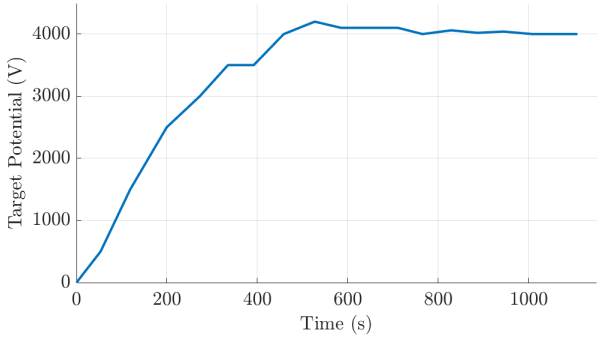

Fig. 9: The target's potential measured using the corrected SEM with active charge control driving the potential to -4000V.

V. Conclusion

The goal of this paper is to develop a controller that actively maintains a desired electrostatic potential on a target by controlling the energy of an electron beam and measuring the target's potential with remote sensing techniques. Using a proportional controller, this goal is achieved for a variety of gains and goal potentials: for gains ranging from 0.2 - 2, the controller converges to a variety of goal potentials with a resolution of at least 50V. For gains less than 1, a resolution of 20V is achieved. From these results, it is shown that remote sensing techniques can be incorporated into the active charge control of a target's potential in a vacuum chamber environment.

Previous active charge control research utilized VUV lamps to discharge the target and drive its potential positive [18]. However, many of the results in this paper present trials where the starting potential of the target is greater than the goal potential. By exploiting the secondary electron behavior, the target can be discharged using only an electron beam and any negative potential can be applied to the target (within the physical limits of the electron gun). For the purpose of the ET, only a negative potential must be applied to the target; therefore only two instruments, the electron beam and

RPA, are necessary, as opposed to the previously believed three instruments [18]. This reduces size, weight, power, and computing requirements for implementing the ET.

While it is expected that the relationship between beam energy and target potential is one-to-one linear, these results show this is not the case. This is likely due to inconsistencies in the impact location of the beam caused by changes in the beam deflection and shape. In spite of these errors, gains are chosen such that the control still converges to the desired goal potential. As long as enough of the beam is impacting the target and secondary electrons are measured, a desired electrostatic potential can be applied to the target. For a spacecraft scenario, precisely determining the impact location of the electron beam on an uncontrolled target is a difficult; therefore, it is beneficial to have a potential control that is robust to pointing errors of the electron beam.

Finally, because the SEM requires a voltage sweep to measure a target's potential, different methods for adjusting the voltage sweep are explored. For potentials greater than 2500V, adjusting the voltage sweep throughout the charging scenario results in control that converges much faster than that of a constant voltage sweep. However, the constant voltage sweep allows a wider range of voltages to be measured accurately at any given time step. The use of either method will depend on the specific parameters of the experiment.

ACKNOWLEDGMENTS

This project was supported by the Department of Defense (DoD) through the National Defense Science and Engineering Graduate (NDSEG) Fellowship Program. Thank you to the Air Force Office of Scientific Research (AFOSR) for general support enabling Electrostatic Tractor research.

REFERENCES

[1] S. T. Lai, *Fundamentals of Spacecraft Charging*. Princeton University Press, Oct. 2011.

[2] K. Wilson and H. Schaub, "Impact of Electrostatic Perturbations on Proximity Operations in High Earth Orbits," *Journal of Spacecraft and Rockets*, vol. 58, no. 5, pp. 1–10, 2021.

[3] ——, "Constrained guidance for spacecraft proximity operations under electrostatic perturbations," in *IEEE Aerospace Engineering Conference*, Big Sky, MT, Mar. 2021, pp. 1–11.

[4] K. T. H. Wilson, 'Alvaro Romero Calvo, and H. Schaub, "Constrained guidance for spacecraft proximity operations under electrostatic perturbations," *Journal of Spacecraft and Rockets*, vol. 59, no. 4, pp. 1304–1316, July–Aug. 2022.

[5] H. Schaub and D. F. Moorer, "Geosynchronous Large Debris Reorbiter: Challenges and Prospects," *The Journal of the Astronautical Sciences*, vol. 59, no. 1-2, pp. 161–176, Jun. 2012.

[6] H. Schaub and Z. Sternovsky, "Active space debris charging for contactless electrostatic disposal maneuvers," *Advances in Space Research*, vol. 43, no. 1, pp. 110–118, 2014.

[7] D. F. Moorer and H. Schaub, "Electrostatic spacecraft reorbiter," 2011a.

[8] ——, "Hybrid electrostatic space," 2011b.

[9] H. Schaub and L. E. Z. Jasper, "Circular orbit radius control using electrostatic actuation for 2-craft configurations," in *AAS/AIAA Astrodynamics Specialist Conference*, Girdwood, Alaska, July 31 – August 4 2011, Paper AAS 11–498.

[10] M. Bengtson, J. Hughes, and H. Schaub, "Prospects and Challenges for Touchless Sensing of Spacecraft Electrostatic Potential Using Electrons," *IEEE Transactions on Plasma Science*, vol. 47, no. 8, pp. 3673–3681, Aug. 2019.

[11] K. Wilson and H. Schaub, "X-Ray Spectroscopy for Electrostatic Potential and Material Determination of Space Objects," *IEEE Transactions on Plasma Science*, vol. 47, no. 8, pp. 3858–3866, Aug. 2019.

[12] A. Pedersen, C. Chapell, K. Knott, and et all, "Methods for keeping a conductive spacecraft near the plasma potential," in *Spacecraft Plasma Interactions and Their Influence on Field and Particle Measurements, Proceedings of the 17th ESLAB Symposium, ESA SP-198*. Citeseer, 1983, pp. 185–190.

[13] R. Schmidt, H. Arends, K. Torkar, and N. Valanvanoglou, *Novel Methods for Active Spacecraft Potential Control*. American Geophysical Union (AGU), 1989, pp. 261–265.

[14] R. Schmidt, H. Arends, A. Pedersen, F. Rüdenauer, and et al, "Results from active spacecraft potential control on the geotail spacecraft," *Journal of Geophysical Research: Space Physics*, vol. 100, no. A9, pp. 17 253–17 259, 1996.

[15] K. Torkar, W. Riedler, C. P. Escoubet, and et al, "Active spacecraft potential control for cluster – implementation and first results," *Ann. Geophys.*, 2001.

[16] K. Torkar, R. Nakamura, and M. Tajmar, "Active spacecraft potential control investigation," *Space Sci Rev*, 2016.

[17] H. Schaub, G. G. Parker, and L. B. King, "Challenges and prospect of coulomb formations," *Journal of the Astronautical Sciences*, vol. 52, no. 1–2, pp. 169–193, Jan.–June 2004.

[18] J. D. Walker and H. Schaub, "Active charge control using an electron beam and ultraviolet light source," in *AIAA Science and Technology Forum and Exposition (SciTech)*, Orlando, FL, Jan. 8–12 2024.

[19] B. Draine and E. Salpeter, "On the physics of dust grains in hot gas," *The Astrophysical Journal*, vol. 231, pp. 77–94, 1979.

[20] J. Hammerl, A. Haft, and H. Schaub, "Neighboring spacecraft charging due to continuous electron beam emission and impact," in *Applied Space Environments Conference*, Oct. 9-13 2023.

[21] K. Wilson, Á. Romero-Calvo, M. Bengtson, J. Hammerl, J. Maxwell, and H. Schaub, "Development and characterization of the ECLIPS space environments simulation facility," *Acta Astronautica*, vol. 194, pp. 48–58, May 2022.

[22] K. T. H. Wilson, M. Bengtson, and H. Schaub, "Remote electrostatic potential sensing for proximity operations: Comparison and fusion of methods," *Journal of Spacecraft and Rockets*, vol. 59, no. 5, pp. 1425–1436, Sept. – Oct. 2022.

[23] M. Bengtson, K. T. H. Wilson, and H. Schaub, "Simulations and experimental results of electron method for remote spacecraft charge sensing," in *Applied Space Environments Conference*, Los Angeles, CA, May 13–17 2019.